Temporal–Spatial Distribution of Atmospheric Predictability Limit by Local Dynamical Analogs

JIANPING LI AND RUIQIANG DING

State Key Laboratory of Numerical Modeling for Atmospheric Sciences and Geophysical Fluid Dynamics (LASG), Institute of Atmospheric Physics, Chinese Academy of Sciences, Beijing, China

(Manuscript received 21 October 2010, in final form 12 April 2011)

ABSTRACT

To quantify the predictability limit of a chaotic system, the authors recently developed a method using the nonlinear local Lyapunov exponent (NLLE). The NLLE method provides a measure of local predictability limit of chaotic systems and is intended to supplement existing predictability methods. To apply the NLLE in studies of actual atmospheric predictability, an algorithm based on local dynamical analogs is devised to enable the estimation of the NLLE and its derivatives using experimental or observational data. Two examples are given to illustrate the effectiveness of the algorithm, involving the Lorenz63 three-variable model and the Lorenz96 forty-variable model; they reveal that the algorithm is applicable in estimating the NLLE of a chaotic system from its experimental time series. On this basis, the NLLE method is used to investigate temporal–spatial distributions of predictability limits of the daily geopotential height and wind fields. The limit of atmospheric predictability varies widely with region, altitude, and season. The predictability limits of the daily geopotential height and wind fields are generally less than 3 weeks in the troposphere, whereas they are approximately 1 month in the lower stratosphere, revealing a potential predictability source for forecasting weather from the stratosphere. Further work is required to examine broader applications of the NLLE method in predictability studies of the atmosphere, ocean, and other systems.

1. Introduction

Since the pioneering works of Thompson (1957) and Lorenz (1963, 1965), atmospheric predictability has been extensively studied based on theoretical, numerical, and statistical models (e.g., Smagorinsky 1969; Leith 1983; Dalcher and Kalnay 1987; Fraedrich 1986, 1987; Chou 1989; Farrell 1990; Simmons et al. 1995; Palmer 2006). It has long been recognized that the upper limit of weather predictability for the synoptic and larger scales is about 2 weeks. This limit gives a general estimate of weather predictability for the global atmosphere. However, atmospheric predictability is largely a function of location and season (González-Miranda 1997; Kumar et al. 2003; Reichler and Roads 2004; Chen et al. 2006), implying that a three-dimensional structure of the predictability limit exists in the global atmosphere. Previous studies have investigated the temporal–spatial distribution of atmospheric predictability (Rowell 1998; Kumar et al. 2003; Reichler and Roads 2004); however, these studies were based primarily on numerical models, for which model deficiencies would have strongly influenced the estimates of atmospheric predictability. Moreover, these studies provided only qualitative estimates of atmospheric predictability, such as information on regions with either higher or lower predictability but no further details. As a result, a method for quantitatively estimating the temporal–spatial distribution of the atmospheric predictability limit needs to be developed.

Observed atmospheric data contain almost all of the real information regarding the day-to-day movement and evolution of weather systems. Given that the precise dynamical equations of atmospheric motion are explicitly unknown, it is more appropriate to investigate quantitatively the temporal–spatial distribution of the atmospheric predictability limit based on observational data. Estimation of atmospheric predictability based on circulation analogs has been discussed in previous studies (Lorenz 1969; Chen 1989; Toth 1991; Trevisan 1995). Lorenz (1969) introduced the so-called natural analogs, over a very large region such as the Northern Hemisphere

Corresponding author address: Jianping Li, LASG, Institute of Atmospheric Physics, Chinese Academy of Sciences, P.O. Box 9804, Beijing 100029, China.
E-mail: ljp@lasg.iap.ac.cn

DOI: 10.1175/MWR-D-10-05020.1

or the globe, which is also termed the global analog or spatial pattern analog, to study global predictability over the globe, a hemisphere, or a large region. According to Van den Dool (1994), it would take a library of order 10^{30} yr to find good global analogs over a large region such as the Northern Hemisphere (where the number of spatial degrees of freedom is large). Obviously, it is impossible to find good global analogs with current libraries of historical atmospheric data (order 10–100 yr). However, over a small enough area (where the number of spatial degrees of freedom is relatively small), the probability of finding good analogs is great with only 10–100 yr of data (Van den Dool 1994). Consequently, it is possible to use current libraries of historical atmospheric data to investigate the local predictability of the atmosphere.

The main purpose of this study is to develop a new method using local dynamical analogs for quantitatively investigating the temporal–spatial distribution of the atmospheric predictability limit. The method is based on the nonlinear local Lyapunov exponent (NLLE), which is a nonlinear generalization to the existing local or finite-time Lyapunov exponents. In the studies of nonlinear dynamical systems, the Lyapunov exponents measure the average exponential rates of divergence or convergence of nearby orbits on a strange attractor and, thus, quantify the average predictability properties of a chaotic system (Oseledec 1968). By definition, if the initial perturbation is of the size δ_0 and if the accepted error tolerance Δ remains small, then the largest Lyapunov exponent $\lambda_{\max}$ provides an estimate of the average predictability time in a chaotic system: $T_p \sim 1/\lambda_{\max} \ln(\Delta/\delta_0)$ (Eckmann and Ruelle 1985; Wolf et al. 1985; Lorenz 1996). Therefore, the largest Lyapunov exponent is an important parameter that characterizes the average predictability of chaotic systems. For systems whose equations of motion are explicitly known, a standard algorithm has been developed for computing the largest Lyapunov exponent (Shimada and Nagashima 1979; Benettin et al. 1980). There also exist several algorithms for calculating the largest Lyapunov exponent from a time series (Sano and Sawada 1985; Wolf et al. 1985).

Whereas the (global) Lyapunov exponent provides a measure of the total predictability of a system, it is sometimes useful to estimate the local predictability around a point x_0 in phase space. Consequently, various local or finite-time Lyapunov exponents have been proposed (Yoden and Nomura 1993; Kazantsev 1999; Ziehmann et al. 2000), for measuring the short-term growth rate of small initial perturbations. However, the existing local or finite-time Lyapunov exponents, which are similar to the global Lyapunov exponents, are established based on the assumption that the initial perturbations are sufficiently small that their evolution can be approximately governed by the tangent linear model (TLM) of a nonlinear system, which essentially belongs to linear error growth dynamics. Clearly, as long as an uncertainty remains infinitesimal within the framework of the linear error growth dynamics, it cannot pose a limit to predictability. Therefore, nonlinear patterns of behavior in error growth should be considered when determining the predictability limit (Lacarra and Talagrand 1988; Mu 2000).

In view of the limitations of linear error growth dynamics, it is necessary to propose a new method based on nonlinear error growth dynamics for quantifying the predictability limit of chaotic systems. Recently, the NLLE has been introduced to study the predictability of an n-dimensional chaotic system or a single variable within the system (Li et al. 2006; Ding and Li 2007; Ding et al. 2008; Li and Ding 2009; Li and Wang 2008). The NLLE measures the average growth rate of the initial errors of nonlinear dynamical models without linearizing the governing equations. The experimental results from Ding and Li (2007) showed that, with the NLLE and its derivatives, the limit of dynamic predictability in large classes of chaotic systems can be efficiently and quantitatively determined. Compared to a linear method, the NLLE is more suitable for determining quantitatively the predictability limit of a chaotic system.

In addition to the NLLE, other definitions based on the fully nonlinear equations, such as the finite-size Lyapunov exponent (FSLE; Aurell et al. 1997; Boffetta et al. 1998), have been introduced and applied to analyses of geophysical flows, yielding interesting results. The NLLE bears some similarities to the FSLE, as both examine the nonlinear error growth of initial errors in order to overcome the limitations of the Lyapunov exponents. However, some differences exist between the NLLE and the FSLE. For example, the FSLE only depends on initial errors, while the NLLE depends not only on initial errors but also on the initial state and evolution time. In addition, the NLLE can be used to measure the averaged growth rate of the initial errors of the entire n-dimensional system and a single variable of the system, whereas the FSLE only measures the average growth rate of the initial errors of the entire n-dimensional system. Most importantly, the NLLE may effectively quantify the predictability limit of chaotic systems, while the FSLE focuses on examining the nonlinear error growth rate of the initial errors.

With regard to the computation of the NLLE, if the system's equations of motion are explicitly known, such as the Lorenz63 model (Lorenz 1963), we can directly obtain the mean NLLE and the mean error growth via numerical integration of the Lorenz63 model and its

error evolution equations (Ding and Li 2007; Ding et al. 2008). However, the atmosphere is an infinite-dimensional system, in which there are many parameters and physical processes that are explicitly unknown. Fortunately, for many systems in reality, we can obtain observational data, although the explicit governing equations of such data are probably unknown. Consequently, it is possible to estimate the NLLE by making use of the observational data available.

In previous studies, if experimental or observational data were available for a single variable of a chaotic system, the method of phase space reconstruction by time delay embedding was then applied in reconstructing the phase space of the system (Sano and Sawada 1985; Wolf et al. 1985; Fraedrich 1986, 1987; Keppenne and Nicolis 1989). To achieve a good reconstruction, two parameters we need to estimate are the time delay and the embedding dimension. The standard method used to determine the time delay is based on automutual information, and that used to determine the embedding dimension is the false nearest-neighbor method (Kantz and Schreiber 1997, 36–39). The Lyapunov exponents are estimated by calculating the mean exponential divergence rate of initially close trajectories in the reconstructed phase space. However, in practical applications many difficulties are encountered in the appropriate selection of the embedding dimension (Holzfuss and Lauterborn 1989; Li and Chou 1996). The estimation of Lyapunov exponents is sensitive to the choice of the embedding dimension. How small or large the embedding dimension is will lead to spurious Lyapunov exponents. These spurious Lyapunov exponents can sometimes be larger than the true Lyapunov exponents, which can then lead to erroneous conclusions of the predictability time of chaotic systems.

In addition, Wolf et al. (1985) pointed out that the required number of experimental or observational data points for accurate calculation of the Lyapunov exponent ranges from 10^d to 30^d, where d is related to the dimension of the attractor. For chaotic systems with rather broad spectra, such as the atmosphere, whose attractor is generally of a very large dimension, one must have a very large amount of observational data for the accurate calculation of the Lyapunov exponent. In fact, current libraries of historical atmospheric data are not large enough to provide such data. Consequently, studies of atmospheric predictability using the method of phase space reconstruction are severely limited by relatively short observational records of the atmosphere, which is similar to the situation using the method of global analogs.

In the present study, as an alternative to the global analog, we introduce a local dynamical analog and develop a new algorithm to search for the local dynamical analog from experimental or observational time series, thereby enabling an estimate of the NLLE. For a small local region or a single grid point, the small number of spatial degrees of freedom makes it possible to find good local dynamical analogs with current libraries of historical atmospheric data (Van den Dool 1994). The new algorithm allows us to search for local dynamical analogs from observational time series, avoiding the phase space reconstruction and thereby eliminating the possibility of generating a spurious estimate of the NLLE. Based on this new algorithm, the NLLE and its derivatives can be used to investigate quantitatively the temporal–spatial distribution of the atmospheric predictability limit. We, therefore, term our entire approach the NLLE method.

It should be pointed out that Chen et al. (2006) described a rather preliminary algorithm to estimate the NLLE and applied the NLLE to study the predictability of the 500-hPa geopotential height field. The NLLE method in this paper presents a substantial improvement and a wider application compared to the findings of Chen et al. (2006). The remainder of this paper is arranged as follows. Section 2 provides a brief description of the NLLE and its application in estimating the predictability limit, and section 3 introduces the algorithm based on local dynamical analogs to estimate the NLLE using experimental or observational data. Section 4 tests the validity of the algorithm by applying it to a simple system, the Lorenz63 model (Lorenz 1963), and to a relatively complex example, the Lorenz96 model (Lorenz 1996). Data requirements and noise problems of the NLLE method are discussed in section 5. Section 6 shows an application of the NLLE method in atmospheric predictability, followed by a summary in section 7.

2. Nonlinear local Lyapunov exponent (NLLE) and predictability limit

a. *NLLE of an* n*-dimensional dynamical system*

Consider a general n-dimensional nonlinear dynamical system whose evolution is governed by

$$\frac{d\mathbf{x}}{dt} = \mathbf{F}(\mathbf{x}), \tag{1}$$

where $\mathbf{x} = [x_1(t), x_2(t), \ldots\ldots, x_n(t)]^{\mathrm{T}}$ is the state vector at time t, the superscript T is the transpose, and $\mathbf{F}$ represents the dynamics. The evolution of a small error $\boldsymbol{\delta} = [\delta_1(t), \delta_2(t), \ldots\ldots, \delta_n(t)]^{\mathrm{T}}$, superimposed on a state $\mathbf{x}$, is governed by the nonlinear equations:

$$\frac{d}{dt}\boldsymbol{\delta} = \mathbf{J}(\mathbf{x})\boldsymbol{\delta} + \mathbf{G}(\mathbf{x}, \boldsymbol{\delta}), \tag{2}$$

where $\mathbf{J}(\mathbf{x})\boldsymbol{\delta}$ are the tangent linear terms and $\mathbf{G}(\mathbf{x}, \boldsymbol{\delta})$ are the high-order nonlinear terms of the error $\boldsymbol{\delta}$. Because of some difficulties in solving the nonlinear problem, most previous studies (e.g., Lorenz 1965; Eckmann and Ruelle 1985; Yoden and Nomura 1993; Kazantsev 1999; Ziehmann et al. 2000) assumed that the initial perturbations were sufficiently small that their evolutions could be approximately governed by the following linear equations:

$$\frac{d}{dt}\boldsymbol{\delta} = \mathbf{J}(\mathbf{x})\boldsymbol{\delta}. \tag{3}$$

However, the evolution of the linear error is characterized by continuous exponential growth, which is not applicable to a description of a process that involves the initial exponential growth of sufficiently small errors to finally achieve saturation (Ding and Li 2007). To determine the limit of predictability, any proposed ''local Lyapunov exponent'' should be defined with respect to the nonlinear behavior of nonlinear dynamical systems. Without a linear approximation, the solutions of Eq. (2) can be obtained by numerically integrating it along the reference solution $\mathbf{x}$ from $t = t_0$ to $t_0 + \tau$:

$$\boldsymbol{\delta}_1 = \boldsymbol{\eta}(\mathbf{x}_0, \boldsymbol{\delta}_0, \tau)\boldsymbol{\delta}_0, \tag{4}$$

where $\boldsymbol{\delta}_1 = \boldsymbol{\delta}(t_0 + \tau), \mathbf{x}_0 = \mathbf{x}(t_0), \boldsymbol{\delta}_0 = \boldsymbol{\delta}(t_0)$, and $\boldsymbol{\eta}(\mathbf{x}_0, \boldsymbol{\delta}_0, \tau)$ is the nonlinear propagator. The NLLE is then defined as

$$\lambda(\mathbf{x}_0, \boldsymbol{\delta}_0, \tau) = \frac{1}{\tau}\ln\frac{\|\boldsymbol{\delta}_1\|}{\|\boldsymbol{\delta}_0\|}, \tag{5}$$

where $\lambda(\mathbf{x}_0, \boldsymbol{\delta}_0, \tau)$ depends in general on the initial state $\mathbf{x}_0$ in phase space, the initial error $\boldsymbol{\delta}_0$, and time τ. The NLLE differs from existing local or finite-time Lyapunov exponents defined based on linear error dynamics (Kazantsev 1999; Yoden and Nomura 1993; Ziehmann et al. 2000), which depend solely on the initial state $\mathbf{x}_0$ and time τ, not on the initial error $\boldsymbol{\delta}_0$. In the double limits of $\|\boldsymbol{\delta}_0\| \to 0$ and $\tau \to \infty$, the NLLE converges to the largest global Lyapunov exponent, $\lambda_{\max}$ (Ding and Li 2007). The ensemble mean NLLE over the global attractor of the dynamical system is given by

$$\begin{aligned}\overline{\lambda}(\boldsymbol{\delta}_0, \tau) &= \int_{\Omega} \lambda(\mathbf{x}_0, \boldsymbol{\delta}_0, \tau)\, d\mathbf{x} \\ &= \langle \lambda(\mathbf{x}_0, \boldsymbol{\delta}_0, \tau)\rangle_N \quad (N \to \infty),\end{aligned} \tag{6}$$

where Ω represents the domain of the global attractor of the system and $\langle\rangle_N$ denotes the ensemble average of samples of sufficiently large size N ($N \to \infty$). The mean relative growth of the initial error (RGIE) can be obtained by

$$\overline{E}(\boldsymbol{\delta}_0, \tau) = \exp[\overline{\lambda}(\boldsymbol{\delta}_0, \tau)\tau]. \tag{7}$$

Using the saturation theorem from Ding and Li (2007), we obtain

$$\overline{E}(\boldsymbol{\delta}_0, \tau) \xrightarrow{p} c \quad (N \to \infty), \tag{8}$$

where $\xrightarrow{p}$ denotes the convergence in probability and c is a constant that depends on the converged probability distribution P of error growth. The constant c can be considered as the theoretical saturation level of $\overline{E}(\boldsymbol{\delta}_0, \tau)$. Once the error growth reaches the saturation level, almost all information on initial states is lost and the prediction becomes meaningless. Using the theoretical saturation level, the limit of the dynamical predictability can be quantitatively determined (Li et al. 2006; Ding and Li 2007). To estimate the maximum predictability time of chaotic systems, the predictability limit is defined as the time at which the error reaches 99% of its saturation level.

b. NLLE of a single variable

The definition of the NLLE in Eq. (5) aims to quantify the local error growth rate of the entire n-dimensional system, and the magnitude of the error vector is measured by the norm of the n-dimensional vector. However, different variables of an n-dimensional chaotic system may have different predictabilities. To quantify the error growth rates and predictabilities of different variables from an n-dimensional chaotic system, we define the NLLE of a single variable, $x_i (i = 1, 2, \ldots\ldots, n)$, based on Eq. (5):

$$\xi_i(\mathbf{x}_0, \boldsymbol{\delta}_0, \tau) = \frac{1}{\tau}\ln\frac{|\delta_i(t_0 + \tau)|}{|\delta_i(t_0)|}. \tag{9}$$

Similarly, the mean NLLE and RGIE of the variable x_i can be obtained as follows:

$$\begin{aligned}\overline{\xi}_i(\boldsymbol{\delta}_0, \tau) &= \int_{\Omega_{x_i}} \xi_i(\mathbf{x}_0, \boldsymbol{\delta}_0, \tau)\, dx_i \\ &= \langle \xi_i(\mathbf{x}_0, \boldsymbol{\delta}_0, \tau)\rangle_N \quad (N \to \infty), \quad \text{and}\end{aligned} \tag{10}$$

$$\overline{\Phi}_i(\boldsymbol{\delta}_0, \tau) = \exp[\overline{\xi}_i(\boldsymbol{\delta}_0, \tau)\tau]. \tag{11}$$

From Eqs. (9)–(11), we obtain

$$\overline{\Phi}_i(\boldsymbol{\delta}_0, \tau) = \exp\left[\frac{1}{N}\sum_{j=1}^{N}\ln\frac{|\delta_{ij}(t_0 + \tau)|}{|\delta_{ij}(t_0)|}\right]. \tag{12}$$

For a given initial error $\delta_i(t_0)$ of variable x_i, we have

$$\overline{\Phi}_i(\boldsymbol{\delta}_0, \tau) = \left[\prod_{j=1}^{N} |\delta_{ij}(t_0+\tau)|\right]^{1/N} \Big/ |\delta_i(t_0)| . \quad (13)$$

For chaotic systems, as $\tau \to \infty$, $|\delta_{i1}(t_0+\tau)|, |\delta_{i2}(t_0+\tau)|, \ldots\ldots, |\delta_{iN}(t_0+\tau)|$ are independent and identically distributed, following

$$f(x) = \begin{cases} p(x), & 0 \le x \le a, \\ 0, & x < 0 \quad \text{or} \quad x > a, \end{cases} \quad (14)$$

where a is a positive constant [because the chaotic attractor is confined to a finite region, a is thought to be the maximum value of $\delta_i(t_0+\tau)$], and $p(x)$ is a continuous function defined over an enclosed interval $[0, a]$. Using the Khinchine's weak law of large numbers (Rose and Smith 2002), as $\tau \to \infty$, in the same way as in Eq. (8), we can prove

$$\overline{\Phi}_i(\boldsymbol{\delta}_0, \tau) \xrightarrow{p} c_i \quad (N \to \infty), \quad (15)$$

where c_i can be considered the theoretical saturation level of $\overline{\Phi}_i[\boldsymbol{\delta}(t_0), \tau]$. Using the theoretical saturation level c_i, the limit of the dynamical predictability of variable x_i can be quantitatively determined. Li and Ding (2009) showed that the predictability limits of different variables in multidimensional chaotic systems are interrelated with each other. The ratio of the predictability limit of a single variable to that of the entire system remains almost constant, regardless of the magnitude of initial errors.

3. An algorithm based on local dynamical analogs to estimate the NLLE from experimental or observational data

As stated above, the NLLE can be determined by Eqs. (5) or (9) if the governing equations of an n-dimensional dynamical system are explicitly known. However, if we only obtain the experimental data of a single variable x of an n-dimensional chaotic system, or observe the atmospheric data of variable x at one point of n spatial grid points [e.g., the time series of x is given by $\{x(t_i), i = 0, 1, 2, \ldots\ldots, m-1\}$ where m represents the length of the time series], the question of how to estimate the NLLE of variable x from the time series is of practical significance. To estimate the NLLE, it is necessary to examine the growth rate of the distance between two initially close states in phase space. Thus, the first step is to seek analogous initial states from the time series. Because only the time series of variable x is available (information is lacking regarding other variables of the n-dimensional system), it is necessary to develop a technique that simply relies on variable x to find local analogous states in the n-dimensional phase space. On the one hand, variable x has a small initial error between two local analogous states; on the other hand, other variables have as small initial errors as possible.

For chaotic systems, the evolutions of two states are sure to be analogous over a short time if they are analogous at the initial time (Lorenz 1969; Wolf et al. 1985). Conversely, it is highly likely that two states are analogous at the initial time if their evolutions in phase space are analogous during the initial stage (i.e., over a short time). By simply relying on the variable x, we can take advantage of this property of chaotic systems to search for local analogous states and to exclude, as much as possible, local nonanalogous states. Without reconstruction of the phase space, the initial information and evolutionary information on the reference trajectory of variable x are used to search for local analogs in space phase. In this way, it is almost impossible to find true analogs in full space or over a very large region. However, it is possible to find good local analogs at a point or over a relatively small region, thereby enabling us to quantitatively estimate the limit of local predictability. This analog is referred to as a "local dynamical analog." An algorithm that allows an estimation of the mean NLLE from the experimental or observational time series of variable x is given as follows.

a. Step 1

Taking $x(t_0)$ as the reference point at time t_0, we first seek the local dynamical analog $x(t_k)$ of the reference point from the dataset. Two distances (i.e., the initial distance between two points and the evolutionary distance between their trajectories within a short initial period) are used to measure the degree of similarity between the points. All points $x(t_j)(|t_j - t_0| > t_D$, where t_D is the time taken for autocorrelations of the variable x to drop to around 0.0, ensuring that a good analog pair is not merely due to persistence) in the dataset form a set S. The initial distance d_i between the points $x(t_0)$ and $x(t_j)$ is given by

$$d_i = |x(t_0) - x(t_j)| . \quad (16)$$

We assume that the evolutions of the two points are analogous over a very short time τ, if they are analogous at the initial time. The choice of the short time interval τ depends on the persistence of the variable x; if the persistence is low, the time over which two initially close points remain analogous is relatively short. The time taken for autocorrelations of variable x to drop to 0.9 can be regarded as a rough estimate of the short time

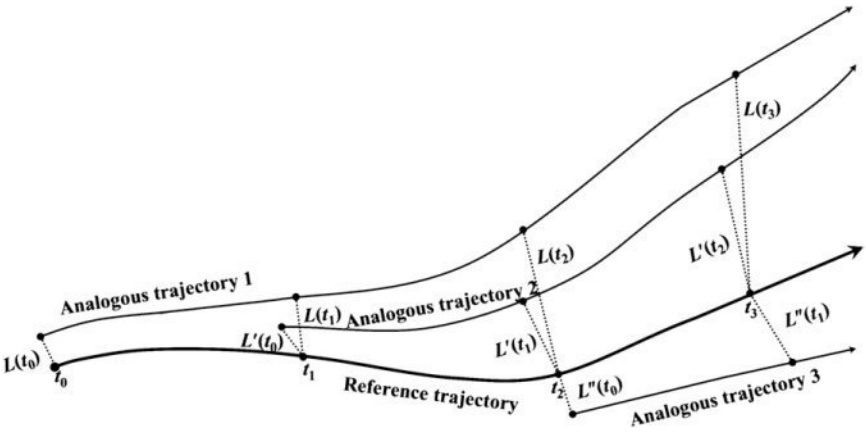

FIG. 1. A schematic representation of the evolution procedure used to estimate the NLLE from experimental or observational data. The evolution trajectory of a local dynamical analog of the reference point at time t_i ($i = 0, 1, 2, \ldots$) is denoted as an analogous trajectory ($i + 1$). The average of the growth rates of the distances between the reference trajectory and all analogous trajectories is used to estimate the NLLE.

interval τ. A high value (0.9) of autocorrelation is chosen to ensure a short time interval (the results were found to be insensitive to the selected value). Within the short interval τ [$\tau = K\Delta$, where Δ is the sampling interval of the time series (i.e., $\Delta = t_i - t_{i-1}$) and K is the ratio of τ to Δ], the evolutionary distance d_e between the two points $x(t_0)$ and $x(t_j)$ is given by

$$d_e = \sqrt{\frac{1}{K+1}\sum_{i=0}^{K}[x(t_i) - x(t_{j+i})]^2}. \tag{17}$$

Here, d_i is the amount of the initial separation between the two points $x(t_0)$ and $x(t_j)$, while d_e is the evolutionary distance between their trajectories over a short initial period. The total distance d_t, considering not only the initial distance but also the evolutionary distance, is found by adding d_i and d_e:

$$d_t = d_i + d_e. \tag{18}$$

If d_t is very small, it is highly likely that the points $x(t_0)$ and $x(t_j)$ are locally dynamically analogous at the initial time.

Of course, this approach is unlikely to exclude the possibility that only the variable x and its most relevant variables remain close, whereas other variables evolve very differently over time, especially for high-dimensional dynamical systems. Therefore, the analogs based on the variable x are only local analogs and that they cannot simply be considered to be global analogs. The constraint of the total distance d_t, which contains both initial information and evolutionary information over a short interval, allows us to exclude a large portion of all points with large initial distances, thereby helping us to find a truly local analog of the reference point.

For every point $x(t_j)$ in the set S, the value of d_t can be determined. The nearest-neighbor (local dynamical analog) $x(t_k)$ of the reference point $x(t_0)$ can be chosen from the set S only if d_t is the minimum. Then, the initial distance between $x(t_0)$ and $x(t_k)$ is denoted as follows:

$$L(t_0) = |x(t_0) - x(t_k)|. \tag{19}$$

b. Step 2

At time $t_i = t_0 + i \times \Delta$ ($i = 1, 2, 3, \ldots\ldots, M$, where M is the total number of time steps), $x(t_0)$ will have evolved to $x(t_i)$ along the reference trajectory, and $x(t_k)$ will have evolved into $x(t_{k+i})$ along the analogous trajectory (Fig. 1). The initial difference $L(t_0)$ will have become

$$L(t_i) = |x(t_i) - x(t_{k+i})|. \tag{20}$$

The growth rate of the initial error during the time interval $(t_i - t_0)$ is

$$\xi_1(t_i) = \frac{1}{t_i - t_0}\ln\frac{L(t_i)}{L(t_0)}. \tag{21}$$

With i gradually increasing, we can obtain the variation of $\xi_1(t_i)$ as a function of the evolution time t_i ($i = 1, 2, 3, \ldots\ldots, M$).

c. Step 3

Taking $x(t_1)$ as the reference state and repeating steps 1 and 2 above (see Fig. 1), we obtain the variation of $\xi_2(t_i)$ as a function of the evolution time t_i.

d. Step 4

The above procedure is repeated until the trajectory reaches the last reference point $x(t_{m-M-1})$. By taking the average of the error growth rates at all reference points, $\{x(t_0), x(t_1), \ldots\ldots, x(t_{m-M-1})\}$, we obtain the mean NLLE:

$$\bar{\xi}(t_i) = \frac{1}{N}\sum_{k=1}^{N} \xi_k(t_i), \quad (i = 1, 2, 3, \ldots\ldots, M), \tag{22}$$

where $N = m - M$ is the total number of reference points on the reference trajectory.

e. Step 5

From Eqs. (21) and (22), we obtain the approximation of the RGIE:

$$\bar{\Phi}(t_i) = \exp[\bar{\xi}(t_i)(t_i - t_0)], \quad (i = 1, 2, 3, \ldots\ldots, M). \tag{23}$$

By investigating the evolution of $\bar{\Phi}(t_i)$ with increasing t_i, we can estimate the mean predictability limit of the variable x.

For systems whose equations of motion are explicitly known, such as the Lorenz63 model, their error growth equations can also be explicitly known. By analyzing the probability distribution of the initial distances between the reference points and their local dynamical analogs using the above algorithm, we find that the initial distances of the variable x follow a lognormal distribution, becoming a Gaussian distribution after a logarithmic transform. Similar results have been found by Gutiérrez et al. (2008) and Primo et al. (2008), who pointed out that the spatial finite perturbations in spatiotemporal chaos follow a lognormal distribution and that they become Gaussian after a logarithmic transform.

By analyzing the Gaussian distribution, we can obtain the initial distance of the variable x with the maximum probability. In step 1 of the algorithm, suppose that the local dynamical analog of the reference point $x(t_0)$ can be found at time t_k, the initial distances of variables other than x in a multivariable system could then be obtained at the same time by calculating the difference between the values at times t_0 and t_k. The initial distances of other variables are also found to follow a lognormal distribution. Hence, the initial distances of other variables with the maximum probability can also be determined. Taking the initial distances of all variables with the maximum probability as the initial perturbations, error growth equations of chaotic systems can yield theoretical results of the NLLE. Finally, we can test the validity of the above algorithm by comparing the experimental results obtained using the algorithm with the theoretical results. If the two results are close and the initial perturbation of variable x with the maximum probability is relatively small, the experimental results obtained using the algorithm are considered meaningful.

4. Case studies

a. The Lorenz63 model

The Lorenz63 model is

$$\begin{cases} dX/dt = -\sigma X + \sigma Y \\ dY/dt = rX - Y - XZ, \\ dZ/dt = XY - bZ \end{cases} \tag{24}$$

where $\sigma = 10$, $r = 28$, and $b = 8/3$, for which the well-known butterfly attractor exists (Lorenz 1963). The time series of variables X, Y, and Z of the Lorenz system can be obtained by using the fourth-order Runge–Kutta method with a time step of $\Delta = 0.01$. The time series includes 8×10^4 points. The error growth equations of the Lorenz63 model are

$$\begin{cases} d\delta X/dt = -\sigma\delta X + \sigma\delta Y \\ d\delta Y/dt = (r - Z)\delta X - \delta Y - (X + \delta X)\delta Z, \\ d\delta Z/dt = (Y + \delta Y)\delta X + X\delta Y - b\delta Z \end{cases} \tag{25}$$

where δX, δY, and δZ are the errors superposed on variables X, Y, and Z, respectively.

Figure 2 shows the probability distribution of the initial distances between the reference points and their local dynamical analogs of variable X. The probability distribution of the initial distances for variables Y and Z can be obtained after the local dynamical analogs of variable X have been found. The initial distances of variables X, Y, and Z with the maximum probability are $e^{-4.2}$, $e^{-3.0}$, and $e^{-2.2}$, respectively. Although the local dynamical analogs of reference points are searched for based on the variable X, the initial distances of variables Y and Z are relatively small compared with their individual standard deviations, indicating that for a very large proportion of reference points their true analogs could be found. By taking $e^{-4.2}$, $e^{-3.0}$, and $e^{-2.2}$ as initial perturbations of variables X, Y, and Z, respectively, the mean error growth of the variable X is obtained via the error growth equations of the Lorenz63 model.

Figure 3a shows two curves that correspond to the mean error growth of the variable X based on the algorithm and the theoretical result from the error growth equations of the Lorenz63 model. The root-mean-square distance (RMSD) between the two curves is

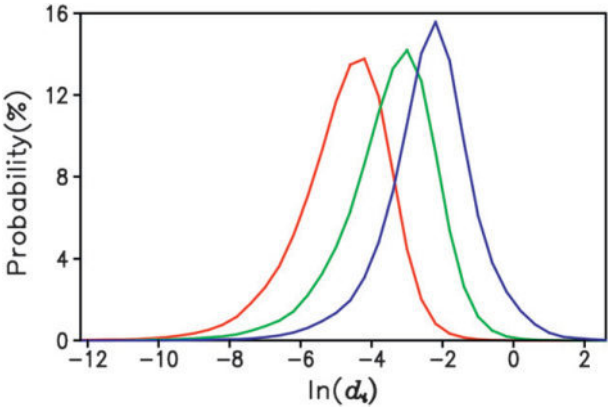

FIG. 2. Probability distributions of the initial distance d_i of variables X (red line), Y (green line), and Z (blue line) from the Lorenz63 model when the local dynamical analogs of reference points are searched for based on the variable X.

$$\text{RMSD} = \sqrt{\sum_{i=1}^{M} (f_i - g_i)^2 \Big/ M},$$

where f_i and g_i are the values of the two curves at each time step, and M is the total number of time steps. The RMSD between the two curves in Fig. 3a is very small (0.11), indicating that the experimental and theoretical results are largely consistent.

Similarly, the mean error growth curves of variables Y and Z based on the algorithm show little difference with the curves of the error growth equations, yielding RMSD values of 0.17 and 0.21, respectively (Figs. 3b and 3c). The results demonstrate that the mean error growth rates of variables X, Y, and Z, as estimated by using the algorithm, closely correspond to the theoretical values derived from the error growth equations. These results verify the validity of the algorithm in determining the mean error growth from the experimental data of a single variable of the Lorenz63 model.

b. *The Lorenz96 model*

The Lorenz63 model is a relatively simple chaotic system with variables that evolve in a low-dimensional attractor. Is the algorithm applicable to more complex, high-dimensional chaotic systems? To answer this question, we chose the Lorenz96 model as an example. The Lorenz96 model (Lorenz 1996) is a 40-variable model that has been used by various authors as a low-order proxy for atmospheric prediction and assimilation studies (e.g., Lorenz and Emanuel 1998; Anderson 2001; Annan 2004). The model has 40 state variables, $X_1, X_2, \ldots, X_{40}$, which are governed by the equation

$$dX_i/dt = (X_{i+1} - X_{i-2})X_{i-1} - X_i + F, \qquad (26)$$

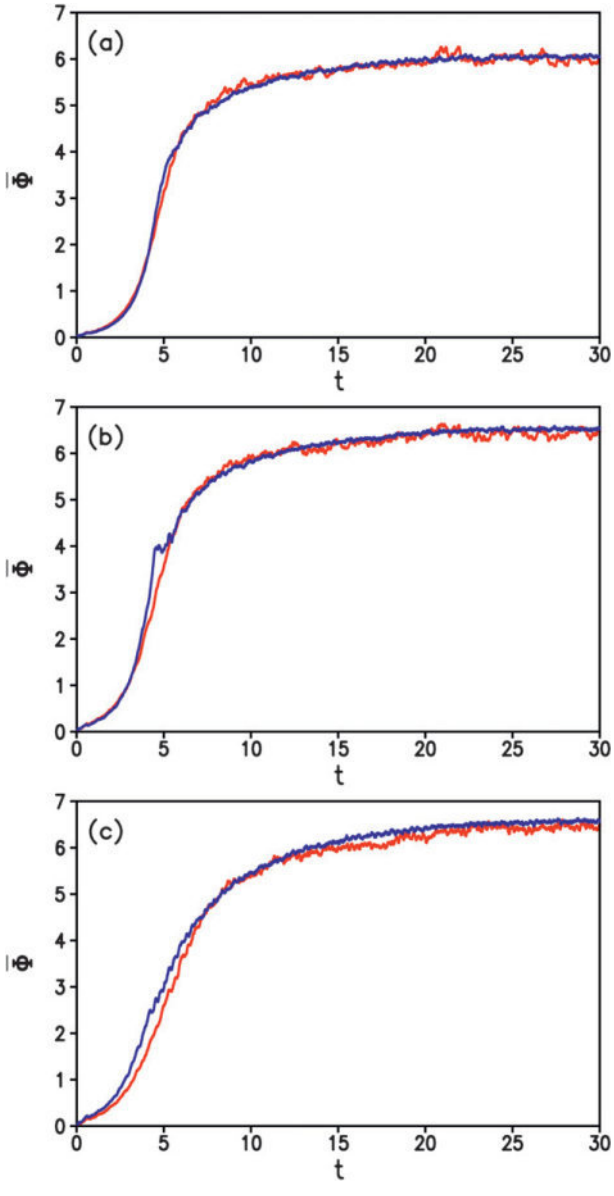

FIG. 3. (a) Mean error growth of variable X of the Lorenz63 model as estimated by the algorithm outlined in section 3 (red line) and the theoretical growth (blue line) from the error growth equations of the Lorenz63 model, in which $e^{-4.2}$, $e^{-3.0}$, and $e^{-2.2}$ are taken as initial perturbations of variables X, Y, and Z, respectively. (b) As in (a), but for variable Y of the Lorenz63 model. (c) As in (a), but for variable Z of the Lorenz63 model. In (a)–(c), $\overline{\Phi}$ denotes the mean error of variables X, Y, and Z, respectively; t denotes time.

where the index $1 \le i \le 40$ is arranged cyclically and F is a fixed forcing. The variables X_i ($1 \le i \le 40$) of the Lorenz96 model may be thought of as values of some atmospheric quantity in 40 sectors of a latitude circle. The model is integrated with the fourth-order Runge–Kutta method with a time step of $\Delta = 0.05$. When $F = 8.0$, the model displays sensitive dependence

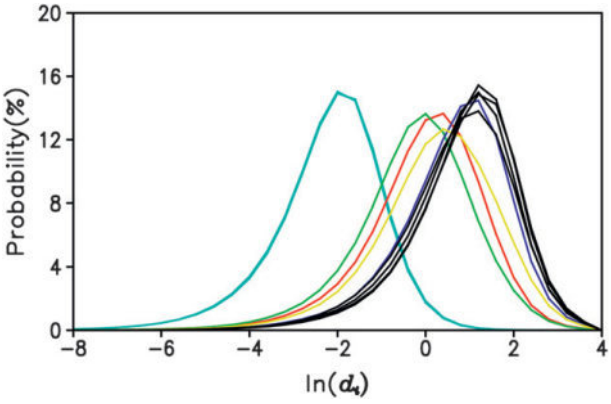

FIG. 4. Probability distributions of the initial distance d_i of variables X_1, X_2, and X_{40} (light blue lines, which overlap with each other and therefore cannot be distinguished), X_3 (red line), X_{39} (green line), X_4 (blue line), X_{38} (yellow line), and X_i ($i = 5, \ldots\ldots, 37$; black lines) of the Lorenz96 model when the local dynamical analogs of reference points are searched for based on the variable X_1.

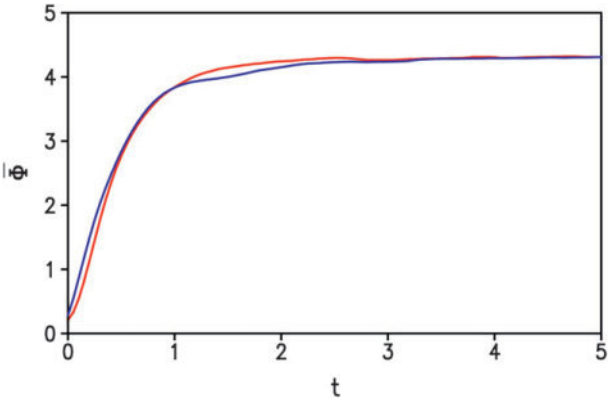

FIG. 5. As in Fig. 3, but for variable X_1 of the Lorenz96 model. In the error growth equations of the Lorenz96 model, $e^{-2.0}$, $e^{0.0}$, $e^{0.4}$, and $e^{0.4}$ are taken as initial perturbations of variables X_1 (and the same for X_2 and X_{40}), X_{39}, X_3, and X_{38}, respectively; other variables X_i ($4 \le i \le 37$) have initial perturbations of $e^{1.2}$.

on the initial conditions. We can obtain the time series of variables X_i ($1 \le i \le 40$) of the Lorenz96 model with the length of $m = 10^5$. The error growth equation of the Lorenz96 model is as follows:

$$d\delta X_i/dt = (\delta X_{i+1} - \delta X_{i-2})X_{i-1} + (X_{i+1} + \delta X_{i+1} - X_{i-2} - \delta X_{i-2})\delta X_{i-1} - \delta X_i, \quad (27)$$

where δX_i is the error on variables X_i ($1 \le i \le 40$). To enhance the information from other variables, the nearest variables X_{i-1} and X_{i+1} of variable X_i are considered when the neighboring points of X_i are searched for using the algorithm. That is, the distance between the reference point $X_i(t_0)$ and the other point $X_i(t_j)$ is replaced by the one between the points $[X_{i-1}(t_0), X_i(t_0), X_{i+1}(t_0)]$ and $[X_{i-1}(t_j), X_i(t_j), X_{i-1}(t_j)]$ as follows:

$$d = \sqrt{\frac{1}{3}[(X_i^0 - X_i^j)^2 + (X_{i-1}^0 - X_{i-1}^j)^2 + (X_{i+1}^0 - X_{i+1}^j)^2]}, \quad (28)$$

where $X_i^0 = X_i(t_0)$, $X_{i-1}^0 = X_{i-1}(t_0)$, $X_{i+1}^0 = X_{i+1}(t_0)$, $X_i^j = X_i(t_j)$, $X_{i-1}^j = X_{i-1}(t_j)$, and $X_{i+1}^j = X_{i+1}(t_j)$. The variable X_i represents the value of some atmospheric quantity in only one sector of a latitude circle. The variables X_{i-1} and X_{i+1} are considered when the local dynamical analogs of X_i are searched for, which is equivalent to a search for the local dynamical analogs of X_i in a larger region.

Figure 4 shows the probability distribution of the initial distances of variables X_i ($1 \le i \le 40$) of the Lorenz96 model when the neighbors of the reference points are searched for based on the variable X_1 (the nearest variables X_2 and X_{40} of X_1 are also included, but are denoted as X_1 for simplicity). It is clear that only X_1 has relatively small initial distances between the reference points and their local dynamical analogs and that the initial distances become larger as the other variables depart further from X_1. The initial distances of variables X_i ($i = 1, 3, 38, 39$) with the maximum probability are $e^{-2.0}$, $e^{0.4}$, $e^{0.4}$, and $e^{0.0}$, respectively, while other variables X_i ($4 \le i \le 37$) have the same initial distance of $e^{1.2}$. This result indicates that only X_1 and its most relevant variables (including X_3, X_{38}, and X_{39}) have small initial perturbations, while the initial perturbations of other variables (including X_i, $4 \le i \le 37$) are relatively large. Certainly, the analogs based on X_1 cannot be called global analogs, and they are only local analogs. According to traditional views of global analogs, these analogs cannot be considered to be good analogs. However, although the mean error of X_1 shows a rapid increase due to the error propagation of other variables, the small initial error of X_1 reaches saturation after some time, suggesting that there still exists a certain predictability limit for this variable (Fig. 5).

If the predictability limit is defined as the time at which the error reaches 99% of its saturation level, the predictability limit of X_1 is determined to be about 30 time steps. Taking the initial distances with the maximum probability as initial perturbations, the mean error growth of X_1, as calculated by the algorithm, is largely consistent with that derived from the error growth equations, with an RMSD of 0.12 for the two curves in Fig. 5. In addition to X_1, the same algorithm is applied to other variables, revealing that the mean error growth of other variables is similar to that of X_1. The predictability limit of other variables is also close to 30 time steps.

Further analysis shows that the predictability limit of each variable, as obtained from the error growth equations of the Lorenz96 model with an initial error of 1.5 on every variable, is about 30 time steps (not shown). Therefore, we infer that the predictability limit of each variable, as deduced using the algorithm, is equivalent to that obtained from the error growth equations with an initial error of 1.5. The standard deviation of each variable of the Lorenz96 model is about 3.0, meaning that the initial error of 1.5 is approximately half of the standard deviation. The results show that the predictability limit of 30 time steps is meaningful, which could be obtained by using only a small initial error based on the error growth equations of the Lorenz96 model.

5. Data requirements and noise

a. Data requirements

Let us now consider an important question on the quantity of experimental or observational data required for an accurate estimation of the predictability limit. The time series of a certain variable should be long enough for identification of truly local analogs at every reference point. The amount of data required to estimate the mean error growth depends on the information of the attractor's probability distribution. With an increasing number of data points, the data will be independent and identically distributed, which follows the attractor's probability distribution (the number of data points $N \to \infty$). If the probability distribution of finite data points (denoted as Q) is close to the attractor's probability distribution (denoted as P), data points can be thought to fill out the structure of the attractor, thereby providing truly local analogous points. Therefore, we can estimate how many points are required by determining if the difference between two probability distributions P and Q remains small. The difference between P and Q is measured by the Kullback–Leibler (KL) divergence (Kullback and Leibler 1951). For P and Q of a discrete random variable, the KL divergence $D_{\mathrm{KL}}(P\|Q)$ of Q from P is defined as

$$D_{\mathrm{KL}}(P\|Q) = \sum_i P(i)\log\frac{P(i)}{Q(i)}. \tag{29}$$

Taking the Lorenz63 model as an example, the probability distribution of variable X obtained by using the number of data points $N = 1 \times 10^6$ (from the fourth-order Runge–Kutta method with a time step of $\Delta = 0.01$) is considered as an approximation of the Lorenz attractor's probability distribution (denoted as P). The probability distribution Q changes with a gradual decrease in the number of data points, as does the KL divergence Q from P, being close to zero for the number of data points $N = 5 \times 10^4 - 9 \times 10^5$ (Fig. 6). When the number of data points has decreased to $N = 1 \times 10^4$, the KL divergence becomes pronounced, indicating that the estimated probability distribution Q of variable X begins to diverge from P. If the KL divergence is less than 0.01 (99%), the number of data points is considered to be the required number of data points. Based on the changes in the KL divergence with different numbers of data points, the minimum number of data points required for estimating the predictability limit of variable X is about 2×10^4.

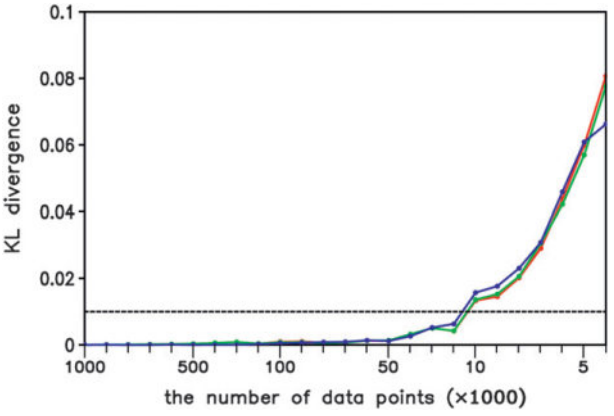

FIG. 6. KL divergence between the probability distributions P and Q of variables X (red line), Y (green line), and Z (blue line) of the Lorenz63 model. Here, P is obtained by using $N = 1 \times 10^6$ data points. The number of data points used to obtain Q varies from 9×10^5 to 4×10^3. The horizontal dashed line shows the KL divergence of 0.01.

Figure 7 shows the estimated predictability limit of variable X as a function of the number of data points. The limit shows a gradual decrease with decreasing number of data points when the number of data points is greater than 2×10^4. However, when the number of data points is less than 2×10^4, the limit shows a rapid decrease with a decreasing number of data points. The estimated predictability limit has an error of approximately 17% when using 2×10^4 data points. For variables Y and Z of the Lorenz63 model, the minimum number of required data points is about 2×10^4 in both cases, similar to that for the variable X (Fig. 6).

In a real situation, the number of experimental or observational data points is finite. The probability distribution Q of experimental or observational data is easily obtained. However, it is impossible to determine the attractor's probability distribution P in advance. Therefore, it is impossible to determine the required number of data points by investigating the KL divergence between P and Q. If the probability distribution of experimental or observational data is assumed to

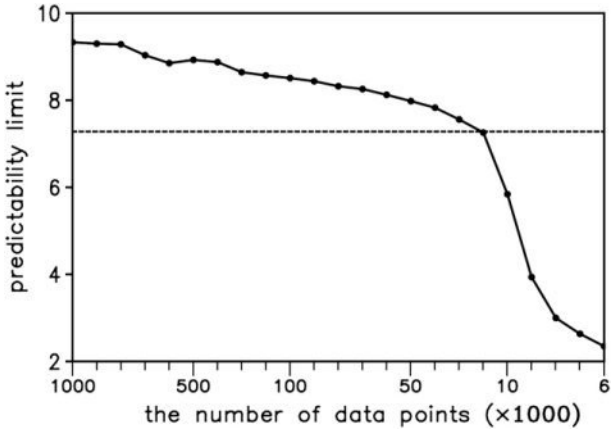

FIG. 7. Estimated predictability limit of variable X of the Lorenz63 model as a function of the number of data points. Because of large fluctuations in error growth when a small number of data points is used, the predictability limit here is defined as the time at which the error reaches 90% of its saturation level, in order to reduce the effects of sampling fluctuations. The dashed line represents the predictability limit obtained using 2×10^4 data points.

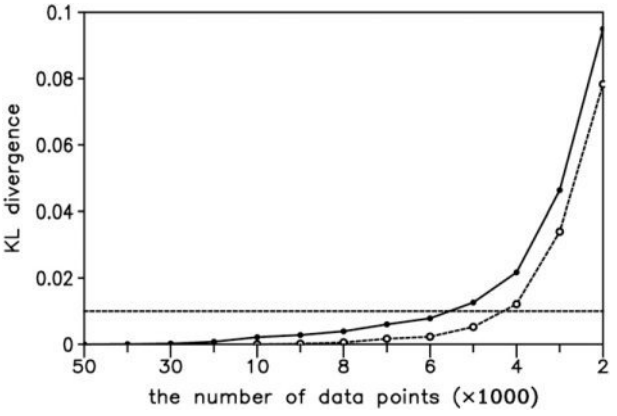

FIG. 8. KL divergence between the probability distributions P and Q of variable X of the Lorenz63 model. The solid line with dots shows the KL divergence, where P is obtained using $N = 5 \times 10^4$ data points, and the number of data points used to obtain Q varies from 4×10^4 to 2×10^3. The dashed line with open circles shows the KL divergence, where P is obtained using $N = 1 \times 10^4$ data points, and the number of data points used to obtain Q varies from 9×10^3 to 2×10^3. The horizontal dashed lines show the KL divergence of 0.01.

be the attractor's probability distribution P, then Q is the probability distribution of a certain portion of the experimental or observational data. Figure 8 shows that when the number of experimental data points of variable X in the Lorenz63 model is large, the KL divergence between P and Q increases slowly at first with a decreasing number of data points. In contrast, when the number of experimental data points is very small, the KL divergence between P and Q shows a rapid increase at first with a decreasing number of data points. Our experimental results indicate that the data would be sufficient to identify good local analogs, if the KL divergence is still less than 0.01 when the number of data points is reduced to 20% of the total number of experimental data points. If the KL divergence does not satisfy this criterion, the estimate of the predictability limit, based on experimental data, would possibly include a large error.

In Fig. 8, when the number of data points is 5×10^4, the KL divergence is still less than 0.01 when the number of data points is reduced to 1×10^4. However, when the number of data points is 1×10^4, the KL divergence is far greater than 0.01 when the number of data points is reduced to 2×10^3. According to the criterion, 5×10^4 (1×10^4) data points of variable X_1 in the Lorenz96 model are sufficient (insufficient) to identify good local analogs. For the Lorenz96 model, 1×10^5 data points are shown to be enough to identify good local analogs, thereby producing a relatively small initial error in X_1 (Fig. 5).

b. Noise

Experimental measurements inevitably contain noise that leads to problems when searching for truly local analogs of reference points. Some false analogs are inevitably found in noise-contaminated experimental or observational data, thereby reducing the estimated predictability limit. Figure 9 shows that when the amplitude of the Gaussian noise exceeds 0.001 σ (where σ is the standard deviation of variable X of the Lorenz63 model), the predictability limit of variable X is greatly reduced. One approach to reducing the effects of noise is

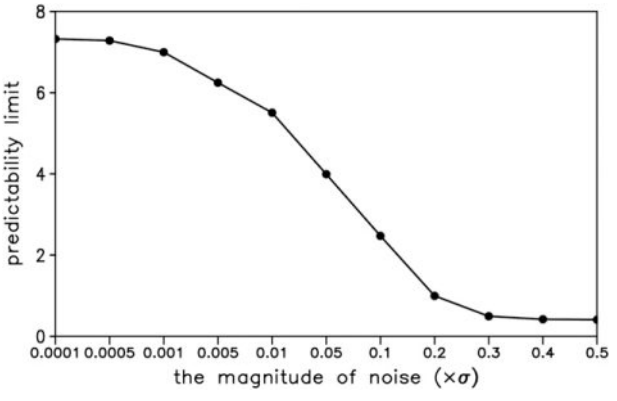

FIG. 9. The estimated predictability limit of variable X of the Lorenz63 model varies with the amplitude of the Gaussian noise. The average value of the Gaussian noise is set to 0 and its standard deviation varies from 0.0001σ to 0.5σ, where σ is the standard deviation of variable X of the Lorenz63 model. Gaussian noise is added to the entire time series of variable X. The predictability limit here is defined in the same way as in Fig. 7, as the time at which the error reaches 90% of its saturation level. The time series of variable X includes 8×10^4 data points.

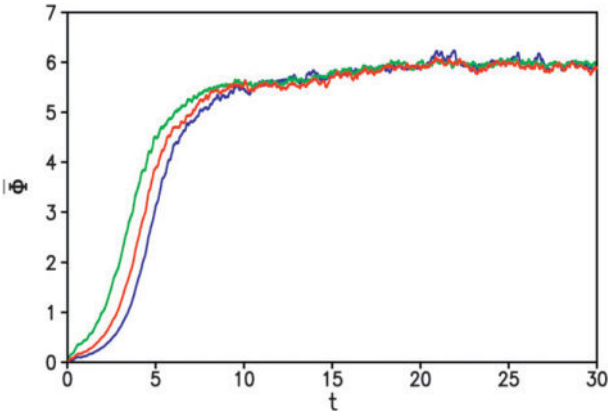

FIG. 10. Estimated error growth of variable X of the Lorenz63 model from a time series with Gaussian noise (green line). The average value of the Gaussian noise is set to 0 and its standard deviation is 0.01σ, where σ is the standard deviation of variable X of the Lorenz63 model. Gaussian noise is added to the entire time series of variable X (total of 8×10^4 data points). The red line shows the estimated error growth of variable X, as derived from a nine-point running mean of the time series with Gaussian noise. The blue line indicates the estimated error growth of variable X from a noise-free time series. Here, $\overline{\Phi}$ denotes the mean error of the variable X and t denotes time.

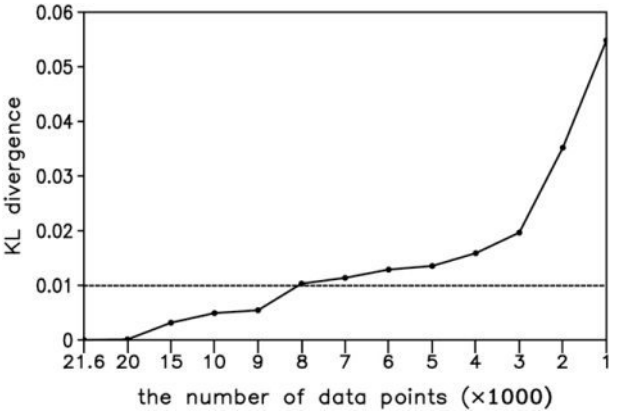

FIG. 11. KL divergence between the probability distributions P and Q of the winter 500-hPa geopotential height at the grid point 40°N, 160°W. Here, P was obtained using $4 \times 90 \times 60 = 21\ 600$ data points. The number of data points used to obtain Q varies from 2×10^4 to 1×10^3. The horizontal dashed line shows the KL divergence of 0.01.

to apply a low-pass filter to the experimental or observational data before estimating the predictability. Filtering can be expected to eliminate noise, but the predictability of the experimental or observational data is not expected to be affected by intensive filtering. Therefore, an appropriate low-pass filtering should be considered to overcome problems associated with noise. A demonstration of filtering (nine-point running mean) for variable X of the Lorenz63 model is shown in Fig. 10. The mean error growth curve obtained from the filtered data is closer (with a smaller RMSD) to the noise-free result than the one obtained from the unfiltered data, indicating that filtering can reduce the effects of noise and improve the estimation of mean error growth. However, if the noise is of sufficiently large amplitude (like 0.1σ), filtering would fail to reduce or eliminate the effects of noise (not shown).

6. Applications of the NLLE method in atmospheric predictability

The NLLE method can be further applied to studies of atmospheric predictability since the global attractor exists in the atmosphere (Li and Chou 1997, 2003; Li and Wang 2008). As is well known, atmospheric observational data show a pronounced annual cycle because of the seasonal march of the sun. Therefore, two points at similar times in different years may have similar dynamical features, probably indicating that the points are close to each other in phase space. We may search for the local dynamical analog of the reference point from all points occurring in a similar "season" in different years (e.g., ±45 days from the reference days for daily observational data). This feature of the atmospheric observation data will help us to find truly analogous points.

Here, we analyze the four-times-daily National Centers for Environmental Prediction–National Center for Atmospheric Research (NCEP–NCAR) reanalysis data (1948–2007). The NCEP–NCAR reanalysis grid has a global spatial coverage of 2.5° latitude × 2.5° longitude, or 144 × 73 grid points. Daily data are obtained as a 1-day moving average of the 4-times-daily data. The time series of every variable at one grid point includes $4 \times 365 \times 60 = 87\ 600$ reference points. Since we use only data of ±45 days in different years from the reference days to search for the analogs, the number of data points available for the analogs is $4 \times 91 \times 59 = 21\ 476$. In Fig. 11, only data from one season (about $4 \times 90 \times 60 = 21\ 600$ data points) is used to examine the KL divergence. The results show that the KL divergence of the winter 500-hPa geopotential height at the grid point 40°N, 160°W is slightly greater than 0.01 when the number of data points is reduced to 20% of the total number of data points. Similar results are obtained at other grid points, indicating that the reanalysis data are barely enough for finding good analogs of local atmospheric patterns.

A single atmospheric variable at a given grid point is denoted as $X_{i,j}$ ($1 \le i \le 144, 2 \le j \le 72$), excluding the North and South Poles. As with the Lorenz96 model, the information of the nearest four grid points around the grid

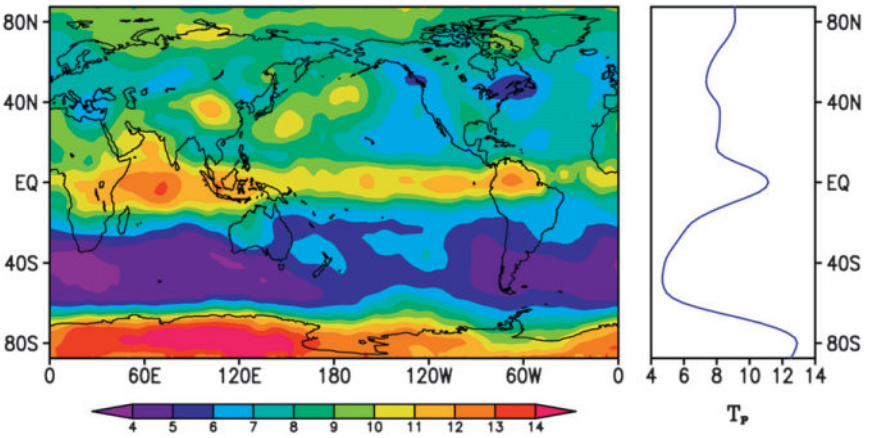

FIG. 12. (left) Spatial distribution of the annual mean predictability limit (in days) of the daily 500-hPa geopotential height field and (right) its zonal mean profile. Here, T_P denotes the predictability limit.

point (i, j) is considered when searching for the local analogs of $X_{i,j}$. The distance in Eq. (28) at the grid point (i, j) is replaced by the one between the reference values and the neighboring values at five neighboring grid points: (i, j), $(i - 1, j)$, $(i + 1, j)$, $(i, j - 1)$, and $(i, j + 1)$. The results indicate that, although the local mean error of the atmospheric variables shows a rapid increase due to the propagation of large initial analogous differences from upstream regions (not shown), good local dynamical analogs ensure the existence of a certain local predictability limit. This limit, caused by local initial analogous errors and error propagation from upstream regions, is useful when investigating the spatial distribution of atmospheric predictability.

Figure 12 shows the spatial distribution of the predictability limit of the daily 500-hPa geopotential height field. The annual mean predictability limit appears to have a zonal distribution, with a maximum of 10–14 days over the tropics and Antarctic, followed by 8–11 days over the Arctic, 6–11 days over the mid- to high latitudes in the Northern Hemisphere, and a lowest limit of 4–6 days at the Southern Hemisphere midlatitudes. In the midlatitudes, baroclinicity is the dominant instability responsible for the growth of small errors at the synoptic (weather) scales. The existence of storm tracks over the midlatitudes explains the minimum predictability limit in these regions, about 5 days at 35°–65°S and 6–8 days at 35°–50°N. However, the situation is somewhat different over the tropics. Baroclinic instability is generally negligible in the tropics, where barotropic and convective instabilities and their interactions are dominant. Reynolds et al. (1994) found that the growth rate of the internal error in the midlatitudes is much greater than that in the tropics, and that model deficiencies are the main error sources in the tropics. Today, the prediction skill of state-of-the-art operational forecast models is close to the predictability limit in the midlatitudes, but far below the predictability limit in the tropics (Bengtsson et al. 2005). The results of the present study suggest that in the tropics a significant increase in prediction skill may be obtained through model improvements, whereas the potential for an increase in prediction skill is much lower in the midlatitudes.

The predictability limit of the daily 500-hPa geopotential height field varies with the season (Fig. 13). In the boreal spring, the predictability limit in the Southern Hemisphere is much higher than that in the Northern Hemisphere; the maximum predictability limit is observed over the Southern Hemisphere subtropics and the Antarctic region. Very low predictability limits in the Southern Hemisphere are seen only in small areas, whereas large areas in the Northern Hemisphere have low limits. In contrast, the predictability limit in the boreal autumn is much higher in the Northern Hemisphere than in the Southern Hemisphere. Over most regions in the Northern Hemisphere, the predictability limit exceeds 9 days, and the maximum predictability limit of about 2 weeks is located mainly in the mid- to low latitudes of the Northern Hemisphere. As we know, weather patterns in autumn are relatively stable, while weather conditions fluctuate strongly in spring, which may explain the higher predictability limit in the autumn hemisphere than in the spring hemisphere.

In the boreal summer, the predictability limit over the tropics and polar regions is relatively high, whereas it is very low in the Northern Hemisphere subtropics and Southern Hemisphere midlatitudes. Compared with the boreal summer, in the boreal winter the predictability limit is high in the Antarctic and over the tropical Indian, North Pacific, and North Atlantic Oceans. The

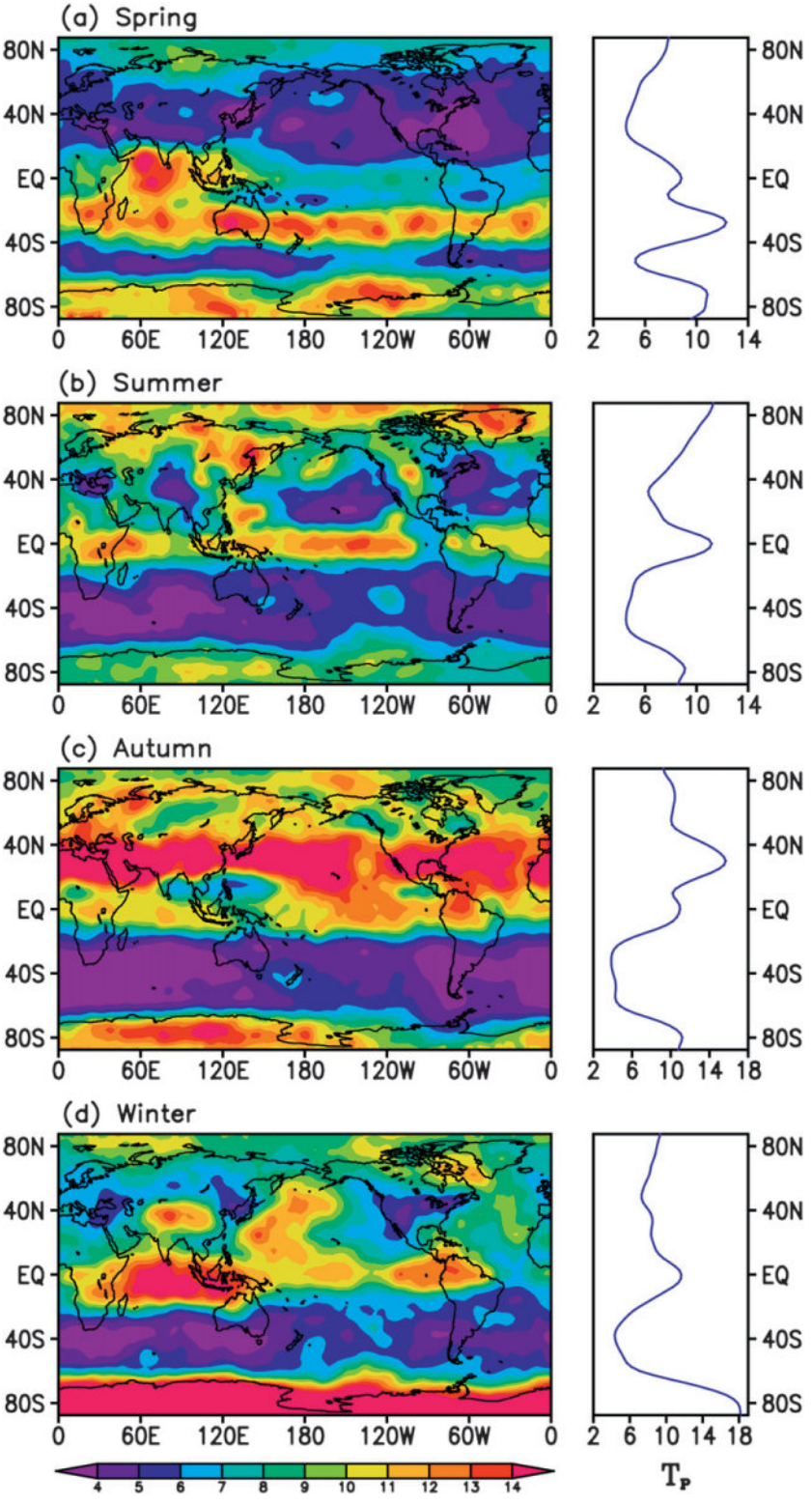

FIG. 13. Spatial distributions of (left) the seasonal mean predictability limit (in days) of the daily 500-hPa geopotential height field and (right) their zonal mean profiles: (a) spring (March–May), (b) summer (June–August), (c) autumn (September–November), and (d) winter (December–February). Here, T_P denotes the predictability limit.

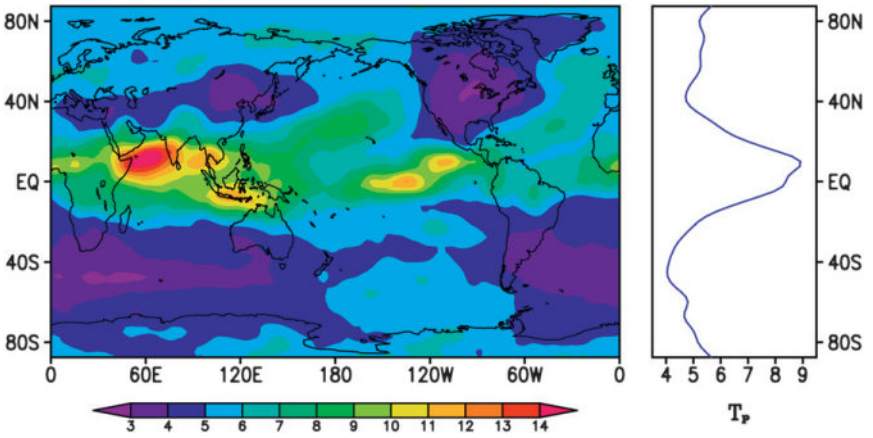

FIG. 14. As in Fig. 12, but for the daily 850-hPa vector wind field. The error of the vector wind field is measured by the absolute error of $\sqrt{(\Delta u)^2 + (\Delta v)^2}$.

existence of good long-range predictability over these regions during the boreal winter was reported by Reichler and Roads (2004), who attributed this finding to the major modes of low-frequency atmospheric variability, including the Southern Hemisphere annular mode (SAM) or Antarctic Oscillation (AAO; Gong and Wang 1999; Thompson and Wallace 2000; Nan and Li 2003), the Pacific–North America teleconnection (PNA; Wallace and Gutzler 1981), and the North Atlantic Oscillation (NAO; Barnston and Livezey 1987; Li and Wang 2003). In addition, there are two belts of low predictability limits located over the midlatitudes of Eurasia and North America in winter, which are largely consistent with the locations of Northern Hemisphere winter storm tracks.

Simmons and Hollingsworth (2002) showed that the European Centre for Medium-Range Weather Forecasts (ECMWF) forecast errors at 500-hPa height over the extratropical Northern Hemisphere during winter 2001 did not reach saturation until 10 days later. However, the predictability limit over most regions of the extratropical Northern Hemisphere in winter is less than 10 days, according to our result shown in Fig. 13d. Our result probably reflects the fact that the propagation of large initial analogous differences in the upstream regions has a significant influence on error growth in downstream regions. On the other hand, atmospheric predictability depends on spatial scales; a large spatial scale generally corresponds to a higher degree of predictability. Therefore, the error averaged over a large region of the extratropical Northern Hemisphere may show slower growth than the error for small regions in the extratropical Northern Hemisphere.

The variability of the wind field is large in the tropics, making it suitable for assessing the predictability limit in the tropics (Bengtsson and Hodges 2006). Figure 14 shows the spatial distribution of the predictability limit of the daily 850-hPa vector wind field. Compared with the daily 500-hPa geopotential height field, the daily 850-hPa vector wind field has a lower predictability limit over most of the globe. The limit is less than 6 days worldwide, except in the tropics, North Pacific, and North Atlantic, where it is beyond 7 days. The predictability limit of the daily 850-hPa vector wind field is the lowest in the mid- to high latitudes of Eurasia, North America, and the Southern Hemisphere, similar to the daily 500-hPa geopotential height field.

The predictability limit of the daily 850-hPa vector wind field also changes with the season (Fig. 15). In the boreal spring, the weather in the Northern Hemisphere is variable and the predictability limit is very low, whereas weather systems in the Southern Hemisphere are stable, resulting in a high predictability limit. The situation in the boreal autumn is the reverse of that in the boreal spring: except off the east coast of Asia and in the northern part of North America, where the predictability limit is below 5 days, the predictability limit throughout the Northern Hemisphere is relatively high, reaching 2 weeks in the North Pacific and North Atlantic. During the boreal autumn, the predictability limit shows large spatial variability in the region from East Asia to the central and eastern Pacific, possibly related to the East Asian trough, which is highly variable, and the subtropical Pacific anticyclone, which is stable. A similar case is found when considering the North American trough over North America and the Azores high over the North Atlantic Ocean. These results may reflect the large differences in local predictability. In fact, local predictability depends on local weather regimes, which have different intrinsic stabilities that determine the spatial variability of local predictability.

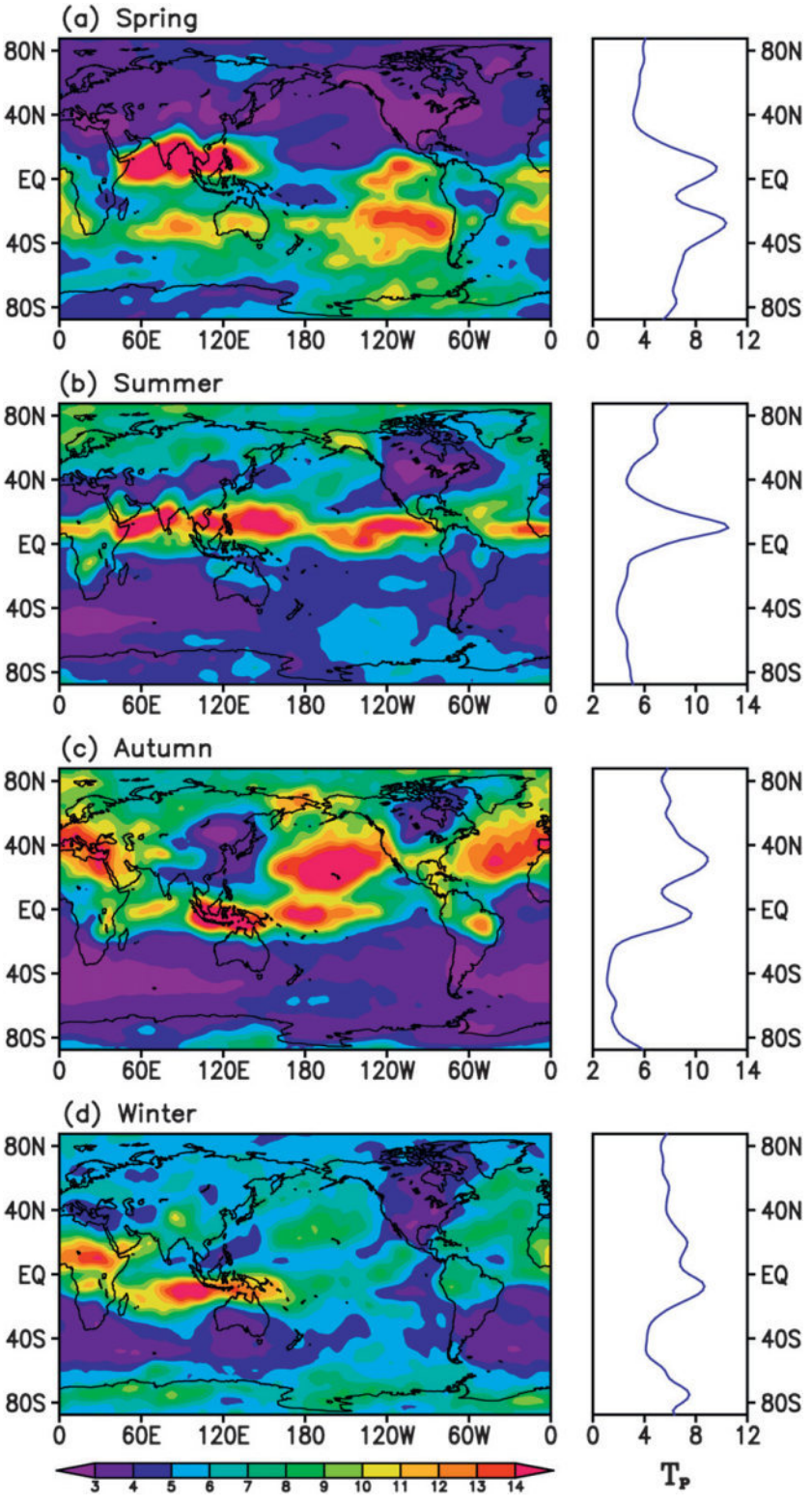

FIG. 15. As in Fig. 13, but for the daily 850-hPa vector wind field.

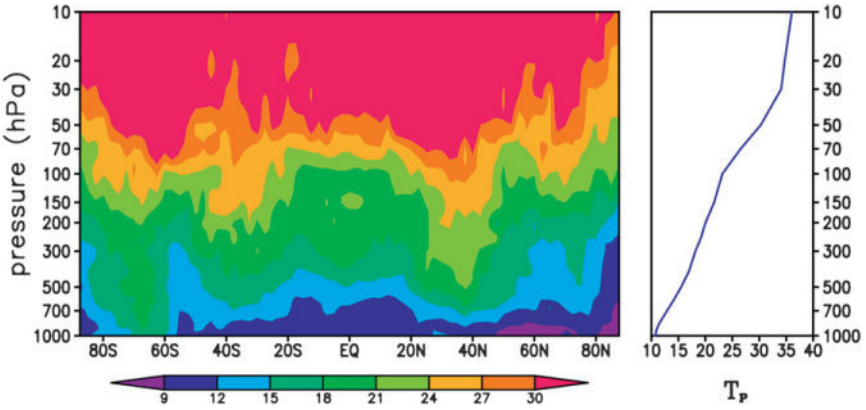

FIG. 16. Vertical distributions of (left) the annual mean predictability limit (in days) of the zonal mean daily geopotential height field and (right) the vertical profile of its meridional mean. Here, T_P denotes the predictability limit.

In the boreal summer, the predictability limit of the daily 850-hPa vector wind field is very high in the western North Pacific, northern Indian, and equatorial eastern Pacific Oceans. Predictions of the daily 850-hPa vector wind field in the western North Pacific are important for forecasting the East Asian summer monsoon. In the boreal winter, the predictability limit of the daily 850-hPa vector wind field is relatively high in the southern tropical Indian, tropical Africa, North Pacific, and North Atlantic Oceans.

We also investigated the vertical distributions of the predictability limit of the daily zonal mean geopotential height and wind fields (Figs. 16 and 17), and found that the predictability limits increase with height for all latitudes. The predictability limit is less than 3 weeks in the troposphere, whereas it is about 1 month in the lower stratosphere. This finding is consistent with the observation that tropospheric weather patterns tend to change on time scales of several days, and that circulation regimes in the stratosphere tend to persist for several weeks or longer (Baldwin and Dunkerton 2001; Baldwin et al. 2003). In the lower stratosphere, the predictability limit of the daily zonal mean vector wind field in the tropics is much higher than that in the mid- to high latitudes in both hemispheres, possibly related to the phenomenon of the quasi-biennial oscillation (QBO; Holton and Lindzen 1972) in the tropical stratosphere. Baldwin et al. (2003) reported that persistent circulation anomalies in the lowermost stratosphere could affect the troposphere through changes to waves in the upper troposphere, which induces surface pressure changes that correspond to the Northern Hemisphere annular mode (NAM). In this way, slow variations of the circulation in the stratosphere may help to increase the skill of extended-range (beyond 10 days) tropospheric weather forecasts. If operational forecast models could adequately resolve the stratosphere–troposphere coupling in the future, the stratosphere may be a potential predictability source for forecasting the extended-range weather in the troposphere.

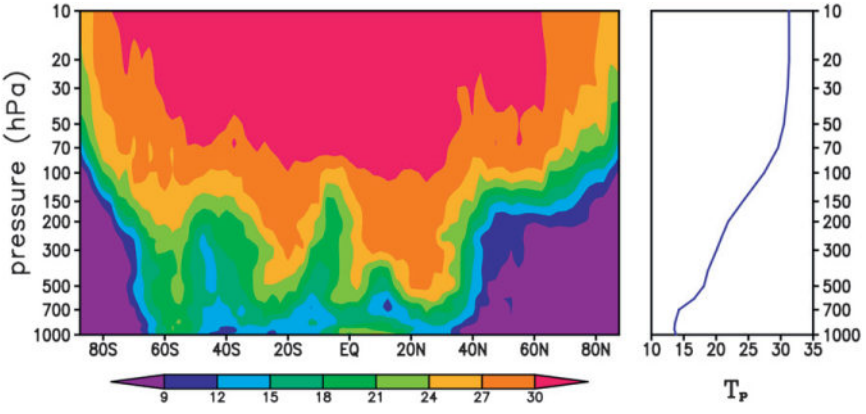

FIG. 17. As in Fig. 16, but for the zonal mean daily vector wind fields.

7. Summary

We have presented a new algorithm that yields estimates of the NLLE and its derivatives from experimental or observational data. The algorithm allows us to search for the local dynamical analogs from experimental or observational time series. By investigating the divergence of the distance between local dynamical analogs, the limit of local predictability may be quantitatively determined. Using the algorithm, we performed a quantitative analysis on temporal–spatial distributions of the predictability limits of the daily geopotential height and wind fields.

For the daily 500-hPa geopotential height field, the limit of weather predictability appears to have a zonal distribution, with a maximum limit of 10–14 days over the tropics and Antarctic, followed by 8–11 days over the Arctic, and 6–11 days over the mid- to high latitudes of the Northern Hemisphere; the lowest limit of 4–6 days is in the Southern Hemisphere midlatitudes. Compared with the daily 500-hPa geopotential height field, the daily 850-hPa vector wind field has a relatively lower predictability limit over most of the globe. The limit is less than 6 days worldwide, except in the tropics, North Pacific, and North Atlantic, where it is beyond 7 days. The predictability limits of the daily 500-hPa geopotential height and 850-hPa vector wind fields vary with season. The predictability limit in autumn is generally higher than that in spring. For most regions in the Antarctic and the tropical Indian, North Pacific, and North Atlantic Oceans, the mean predictability limit in winter is much higher than that in summer. The vertical distributions of the predictability limits of the daily geopotential height and wind fields show an increase in their predictability limits with height. The fact that the predictability limits of the two daily variables are less than 3 weeks in the troposphere and are about 1 month in the lower stratosphere indicates that the stratosphere may be used as a potential predictability source.

Acknowledgments. We thank Prof. M. Mu for many useful comments and assistance with this work. We also thank two anonymous reviewers for their valuable comments that helped to improve the manuscript. Funding for this research was provided jointly by the 973 Program (2010CB950400) and two NSF China projects (40805022 and 40821092).

REFERENCES

Anderson, J. L., 2001: An ensemble adjustment Kalman filter for data assimilation. *Mon. Wea. Rev.,* **129,** 2884–2902.

Annan, J. D., 2004: On the orthogonality of bred vectors. *Mon. Wea. Rev.,* **132,** 843–849.

Aurell, E., G. Boffetta, A. Crisanti, G. Paladin, and A. Vulpiani, 1997: Predictability in the large: An extension of the concept of Lyapunov exponent. *J. Phys.,* **30A,** doi:10.1088/0305-4470/30/1/003.

Baldwin, M. P., and T. J. Dunkerton, 2001: Stratospheric harbingers of anomalous weather regimes. *Science,* **294,** 581–584.

——, and Coauthors, 2003: Stratospheric memory and skill of extended-range weather forecasts. *Science,* **301,** 636–640.

Barnston, G., and R. E. Livezey, 1987: Classification, seasonality and low-frequency atmospheric circulation patterns. *Mon. Wea. Rev.,* **115,** 1083–1126.

Benettin, G., L. Galgani, A. Giorgilli, and J. M. Strelcyn, 1980: Lyapunov characteristics exponents for smooth dynamical systems and for Hamiltonian systems; a method for computing all of them. *Meccanica,* **15,** 9–20.

Bengtsson, L., and K. I. Hodges, 2006: A note on atmospheric predictability. *Tellus,* **58A,** 154–157.

——, ——, and L. S. R. Froude, 2005: Global observations and forecast skill. *Tellus,* **57A,** 515–527.

Boffetta, G., P. Giuliani, G. Paladin, and A. Vulpiani, 1998: An extension of the Lyapunov analysis for the predictability problem. *J. Atmos. Sci.,* **55,** 3409–3416.

Chen, B. H., J. P. Li, and R. Q. Ding, 2006: Nonlinear local Lyapunov exponent and atmospheric predictability research. *Sci. Chin.,* **49D,** 1111–1120.

Chen, W. Y., 1989: Estimate of dynamical predictability from NMC DERF experiments. *Mon. Wea. Rev.,* **117,** 1227–1236.

Chou, J. F., 1989: Predictability of the atmosphere. *Adv. Atmos. Sci.,* **6,** 335–346.

Dalcher, A., and E. Kalnay, 1987: Error growth and predictability in operational ECMWF forecasts. *Tellus,* **39A,** 474–491.

Ding, R. Q., and J. P. Li, 2007: Nonlinear finite-time Lyapunov exponent and predictability. *Phys. Lett.,* **364A,** 396–400.

——, ——, and K. J. Ha, 2008: Nonlinear local Lyapunov exponent and quantification of local predictability. *Chin. Phys. Lett.,* **25,** 1919–1922.

Eckmann, J. P., and D. Ruelle, 1985: Ergodic theory of chaos and strange attractors. *Rev. Mod. Phys.,* **57,** 617–656.

Farrell, B. F., 1990: Small error dynamics and the predictability of atmospheric flows. *J. Atmos. Sci.,* **47,** 2409–2416.

Fraedrich, K., 1986: Estimating the dimensions of weather and climate attractors. *J. Atmos. Sci.,* **43,** 419–432.

——, 1987: Estimating weather and climate predictability on attractors. *J. Atmos. Sci.,* **44,** 722–728.

Gong, D., and S. Wang, 1999: Definition of Antarctic oscillation index. *Geophys. Res. Lett.,* **26,** 459–462.

González-Miranda, J. M., 1997: Predictability in the Lorenz low-order general atmospheric circulation model. *Phys. Lett.,* **233A,** 347–354.

Gutiérrez, J. M., C. Primo, M. A. Rodríguez, and J. Fernández, 2008: Spatiotemporal characterization of ensemble prediction systems the mean variance of the logarithms (MVL) diagram. *Nonlinear Processes Geophys.,* **15,** 109–114.

Holton, J. R., and R. S. Lindzen, 1972: An updated theory for the quasi-biennial oscillation of the tropical stratosphere. *J. Atmos. Sci.,* **29,** 1076–1080.

Holzfuss, J., and W. Lauterborn, 1989: Lyapunov exponents from a time series of acoustic chaos. *Phys. Rev.,* **39A,** 2146–2152.

Kantz, H., and T. Schreiber, 1997: *Nonlinear Time Series Analysis*. Cambridge University Press, 388 pp.

Kazantsev, E., 1999: Local Lyapunov exponents of the quasi-geostrophic ocean dynamics. *Appl. Math. Comput.,* **104,** 217–257.

Keppenne, C. L., and C. Nicolis, 1989: Global properties and local structure of the weather attractor over western Europe. *J. Atmos. Sci.,* **46,** 2356–2370.

Kullback, S., and R. A. Leibler, 1951: On information and sufficiency. *Ann. Math. Stat.,* **22,** 79–86.

Kumar, A., S. D. Schubert, and M. S. Suarez, 2003: Variability and predictability of 200-mb seasonal mean heights during summer and winter. *J. Geophys. Res.,* **108,** 4169, doi:10.1029/2002JD002728.

Lacarra, J. F., and O. Talagrand, 1988: Short-range evolution of small perturbations in a barotropic model. *Tellus,* **40A,** 81–95.

Leith, C. E., 1983: Predictability in theory and practice. *Large-Scale Dynamical Processes in the Atmosphere,* B. J. Hoskins and R. P. Pearce, Eds., Academic Press, 365–383.

Li, J. P., and J. F. Chou, 1996: Some problems existed in estimating fractal dimension of attractor with one-dimensional time series (in Chinese with English abstract). *Acta Meteor. Sin.,* **54,** 312–323.

——, and ——, 1997: Existence of atmosphere attractor. *Sci. Chin.,* **40D,** 215–224.

——, and ——, 2003: Global analysis theory of climate system and its applications. *Chin. Sci. Bull.,* **48,** 1034–1039.

——, and J. X. L. Wang, 2003: A new North Atlantic Oscillation index and its variability. *Adv. Atmos. Sci.,* **20,** 661–676.

——, and S. Wang, 2008: Some mathematical and numerical issues in geophysical fluid dynamics and climate dynamics. *Commun. Comput. Phys.,* **3,** 759–793.

——, and R. Q. Ding, 2009: Studies of predictability of single variable from multi-dimensional chaotic dynamical system (in Chinese with English abstract). *Chin. J. Atmos. Sci.,* **33,** 551–556.

——, ——, and B. H. Chen, 2006: Review and prospect on the predictability study of the atmosphere. *Review and Prospects of the Developments of Atmosphere Sciences in Early 21st Century,* China Meteorology Press, 96–104.

Lorenz, E. N., 1963: Deterministic nonperiodic flow. *J. Atmos. Sci.,* **20,** 130–141.

——, 1965: A study of the predictability of a 28-variable atmospheric model. *Tellus,* **17,** 321–333.

——, 1969: Atmospheric predictability as revealed by naturally occurring analogues. *J. Atmos. Sci.,* **26,** 636–646.

——, 1996: Predictability: A problem partly solved. *Proc. Seminar on Predictability,* Vol. I, Reading, United Kingdom, ECMWF, 1–18.

——, and K. A. Emanuel, 1998: Optimal sites for supplementary weather observations: Simulation with a small model. *J. Atmos. Sci.,* **55,** 399–414.

Mu, M., 2000: Nonlinear singular vectors and nonlinear singular values. *Sci. Chin.,* **43D,** 375–385.

Nan, S. L., and J. P. Li, 2003: The relationship between summer precipitation in the Yangtze River valley and the boreal spring Southern Hemisphere annular mode. *Geophys. Res. Lett.,* **30,** 2266, doi:10.1029/2003GL018381.

Oseledec, V. I., 1968: A multiplicative ergodic theorem: Lyapunov characteristic numbers for dynamical systems. *Trans. Moscow Math. Soc.,* **19,** 197–231.

Palmer, T. N., 2006: Predictability of weather and climate: From theory to practice. *Predictability of Weather and Climate,* T. Palmer and R. Hagedorn, Eds., Cambridge University Press, 1–10.

Primo, C., M. A. Rodríguez, and J. M. Gutiérrez, 2008: Logarithmic bred vectors. A new ensemble method with adjustable spread and calibration time. *J. Geophys. Res.,* **113,** D05116, doi:10.1029/2007JD008998.

Reichler, T., and J. O. Roads, 2004: Time–space distribution of long-range atmospheric predictability. *J. Atmos. Sci.,* **61,** 249–263.

Reynolds, C. A., P. J. Webster, and E. Kalnay, 1994: Random error growth in NMC's global forecast corrections. *Mon. Wea. Rev.,* **122,** 1281–1305.

Rose, C., and M. D. Smith, 2002: *Mathematical Statistics with Mathematica*. Springer-Verlag, 311 pp.

Rowell, D. P., 1998: Assessing potential seasonal predictability with an ensemble of multidecadal GCM simulations. *J. Climate,* **11,** 109–120.

Sano, M., and Y. Sawada, 1985: Measurement of the Lyapunov spectrum from a chaotic time series. *Phys. Rev. Lett.,* **55,** 1082–1085.

Shimada, I., and T. Nagashima, 1979: A numerical approach to ergodic problem of dissipative dynamical systems. *Prog. Theor. Phys.,* **61,** 1605–1616.

Simmons, A. J., and A. Hollingsworth, 2002: Some aspects of the improvement in skill of numerical weather prediction. *Quart. J. Roy. Meteor. Soc.,* **128,** 647–677.

——, R. Mureau, and T. Petroliagis, 1995: Error growth and estimates of predictability from the ECMWF forecasting system. *Quart. J. Roy. Meteor. Soc.,* **121,** 1739–1771.

Smagorinsky, J., 1969: Problems and promises of deterministic extended range forecasting. *Bull. Amer. Meteor. Soc.,* **50,** 286–312.

Thompson, D. W. J., and J. M. Wallace, 2000: Annular modes in the extratropical circulation. Part I: Month-to-month variability. *J. Climate,* **13,** 1000–1016.

Thompson, P. D., 1957: Uncertainty of initial state as a factor in the predictability of large-scale atmospheric flow pattern. *Tellus,* **9,** 275–295.

Toth, Z., 1991: Estimation of atmospheric predictability by circulation analogs. *Mon. Wea. Rev.,* **119,** 65–72.

Trevisan, A., 1995: Statistical properties of predictability from atmospheric analogs and the existence of multiple flow regimes. *J. Atmos. Sci.,* **52,** 3577–3592.

Van den Dool, H. M., 1994: Searching for analogues, how long must we wait? *Tellus,* **46A,** 314–324.

Wallace, J. M., and D. Gutzler, 1981: Teleconnections in the geopotential height field during the Northern Hemisphere winter. *Mon. Wea. Rev.,* **109,** 784–812.

Wolf, A., J. B. Swift, H. L. Swinney, and J. A. Vastano, 1985: Determining Lyapunov exponents from a time series. *Physica D,* **16,** 285–317.

Yoden, S., and M. Nomura, 1993: Finite-time Lyapunov stability analysis and its application to atmospheric predictability. *J. Atmos. Sci.,* **50,** 1531–1543.

Ziehmann, C., L. A. Smith, and J. Kurths, 2000: Localized Lyapunov exponents and the prediction of predictability. *Phys. Lett.,* **4A,** 237–251.